Suppressing the Loss of Ultracold Molecules Via the Continuous Quantum Zeno Effect

B. Zhu,[1] B. Gadway,[1] M. Foss-Feig,[2] J. Schachenmayer,[1] M. L. Wall,[1] K. R. A. Hazzard,[1] B. Yan,[1] S. A. Moses,[1] J. P. Covey,[1] D. S. Jin,[1] J. Ye,[1] M. Holland,[1] and A. M. Rey[1,*]

[1]*JILA, NIST, Department of Physics, University of Colorado, 440 UCB, Boulder, Colorado 80309, USA*

[2]*JQI, NIST, Department of Physics, University of Maryland, College Park, Maryland 20742, USA*

(Received 3 October 2013; published 20 February 2014)

We investigate theoretically the suppression of two-body losses when the on-site loss rate is larger than all other energy scales in a lattice. This work quantitatively explains the recently observed suppression of chemical reactions between two rotational states of fermionic KRb molecules confined in one-dimensional tubes with a weak lattice along the tubes [Yan *et al.*, Nature (London) **501**, 521 (2013)]. New loss rate measurements performed for different lattice parameters but under controlled initial conditions allow us to show that the loss suppression is a consequence of the combined effects of lattice confinement and the continuous quantum Zeno effect. A key finding, relevant for generic strongly reactive systems, is that while a single-band theory can qualitatively describe the data, a quantitative analysis must include multiband effects. Accounting for these effects reduces the inferred molecule filling fraction by a factor of 5. A rate equation can describe much of the data, but to properly reproduce the loss dynamics with a fixed filling fraction for all lattice parameters we develop a mean-field model and benchmark it with numerically exact time-dependent density matrix renormalization group calculations.

DOI: 10.1103/PhysRevLett.112.070404 PACS numbers: 03.65.Xp, 37.10.Jk, 37.10.Pq, 67.85.-d

Ultracold molecules have tremendous applications ranging from quantum many-body physics [1–3] and quantum information processing [4] to precision measurements [5] and ultracold chemistry [6]. However, fast inelastic two-body losses—as occur for KRb with exothermic chemical reactions—can limit molecule lifetimes [7–9], and have been considered a fundamental limitation. Recent experiments with KRb molecules [10] have reported an inhibition of losses when the molecules are confined in an array of one-dimensional tubes with a superimposed axial optical lattice along the tubes (Fig. 1). Similar loss suppression by strong dissipation was previously observed in bosonic Feshbach molecules [11]. Extending the molecules' lifetime over time scales much longer than those determined by tunneling opens a path for the exploration of itinerant magnetism and other many-body phenomena arising from the interplay between dipolar interactions and motion, even in these highly reactive systems.

Free KRb molecules react rapidly. In a lattice, the two-body inelastic collision rates are larger than all other lattice energy scales, including the band separation energy. Consequently, this system is an example of a strongly correlated system that defies simple treatment in terms of single-particle physics. As such, description of the loss suppression based on the assumption that inelastic interactions do not affect the single-particle wave functions is incorrect [12]. Evidence of this issue was reported in Ref. [10] where a heuristic "single-band" treatment of the losses was found to significantly overestimate the molecule filling fraction f.

In this Letter, we develop a theoretical description of the dissipative dynamics that nonperturbatively includes three-dimensional multiband effects. Our analysis allows us to attribute the observed loss suppression to the continuous quantum Zeno effect [13–17]—a suppression of coherent transitions due to strong dissipation—and to generalize previous single-band treatments [17,18] to the strongly dissipative regime. We perform systematic measurements of the KRb lifetime under controlled and reproducible lattice conditions that allow us to validate the calculations. The observed dependence of the loss rate on lattice parameters is consistent with Ref. [10] and is fully reproduced by the multiband theory. Moreover, the inclusion of multiple bands reduces the determined filling f by a factor of ~ 5, giving results consistent with the filling

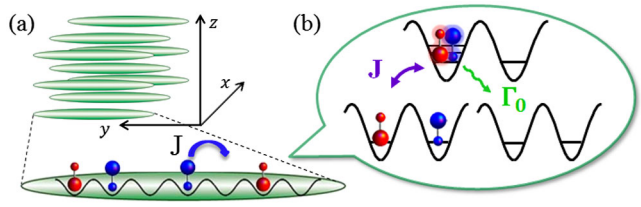

FIG. 1 (color online). (a) A 50:50 mixture of fermionic KRb molecules in two rotational states, $|0,0\rangle$ and $|1,-1\rangle$ (indicated by different colors and shapes), is prepared in a deep 3D lattice, which is suddenly made shallow along one dimension (y). Along y, molecules tunnel with a rate $J/\hbar$ and have a large on-site loss rate Γ_0 because of chemical reactions. (b) In the Zeno regime, $\hbar\Gamma_0 \gg J$, doubly occupied sites are only virtually populated, and the loss occurs at a significantly slower rate $\Gamma_{\rm eff} \ll \Gamma_0$ for molecules on adjacent sites. For KRb, a multiband analysis of this process is required for all experimental lattice parameters.

predicted by Ramsey spectroscopy measurements of molecules pinned in a 3D lattice and prepared under similar initial conditions [10,19].

The multiband calculations are first applied to derive a simple rate equation (RE) for two-body losses, which assumes instantaneous redistribution of molecules between collision events. We show that the RE can describe the measured dissipative dynamics fairly well over a broad range of lattice parameters, but fails for the deepest lattice configurations. We develop a simple and unified theory capable of describing the loss dynamics in *all* parameter regimes based on a mean-field (MF) approximation of the many-body master equation. We validate the MF formulation by comparing it to a numerically exact time-dependent density matrix renormalization group method (t-DMRG) [20–22], which we combine with a quantum trajectory technique [23–25]. The MF, t-DMRG, and experimentally observed loss dynamics quantitatively agree.

Experiment.— The experiment begins by loading $\sim 10^4$ fermionic KRb rovibrational ground-state molecules, $|N = 0, m_N = 0\rangle$, into the lowest band of a deep 3D cubic optical lattice with lattice constant $a = 532$ nm. Here, N is the principal rotational quantum number and m_N is the projection onto the quantization axis, which in our case is determined by an external magnetic field angled 45° between the x and y lattice directions. We next apply a $\pi/2$ microwave pulse to rotationally excite half of the molecules to $|N = 1, m_N = -1\rangle$. We consider $|0, 0\rangle$ and $|1, -1\rangle$ as $|\downarrow\rangle$ and $|\uparrow\rangle$ components of a pseudo-spin 1/2 system. We choose the lattice polarizations so that the tensor ac polarizabilities of $|0, 0\rangle$ and $|1, -1\rangle$ are similar [26]. However, a residual differential ac Stark shift introduces single-particle dephasing that results in a spin-coherence time for the entire sample of ~ 1 ms. This dephasing allows us to prepare an incoherent 50:50 spin mixture of $|\downarrow\rangle$ and $|\uparrow\rangle$ by holding the molecules in the deep lattice for 50 ms. Losses are then initiated by quickly ramping down the lattice depth in the y direction (within 1 ms) to allow tunneling. We measure the number of remaining molecules $|\downarrow\rangle$, i.e., $N_\downarrow(t)$, as a function of the subsequent holding time in the lattice.

We experimentally determine the initial loss rate κ by fitting $N_\downarrow(t)$ to the solution of a two-body loss RE of the form

$$\frac{dN_\downarrow}{dt} = -\frac{\kappa}{N_\downarrow(0)}[N_\downarrow(t)]^2, \tag{1}$$

with $N_\downarrow(0)$ the initial number of $|\downarrow\rangle$ molecules. A typical experimental fit is shown in Fig. 2(a). To avoid the saturation of the losses that originates from the finite number of molecules per tube (~ 6 per tube on average), which cannot be captured by the RE, we fit only up to times when $\sim 25\%$ of the molecules are lost (see Supplemental Material [27]).

The loss rate κ in general depends on the tunneling rate $J/\hbar$ and the on-site "bare" loss rate Γ_0. If a single-band approximation is used, the on-site bare loss rate Γ_0 is given by [17]

$$\Gamma_0 = \beta^{(3D)} \int |W(\mathbf{x})|^4 d^3\mathbf{x}, \tag{2}$$

where $W(\mathbf{x})$ is the lowest-band single-particle 3D Wannier orbital. The two-body loss rate coefficient for molecules in $|0, 0\rangle$ and $|1, -1\rangle$, $\beta^{(3D)}$, was measured to be $\beta^{(3D)} = 9.0(4) \times 10^{-10}$ cm^3 s^{-1} [10].

To experimentally extract the dependence of κ on Γ_0 and the single-particle hopping energy J, we perform similar measurements to those reported in Ref. [10]. However, here we ensure reproducibility of the initial conditions to fix f for all lattice conditions. To measure the Γ_0 dependence we set $V_y = 5E_R$, which fixes J, and then tune Γ_0 by modifying $V_\perp$ [Fig. 2(b)]. Here, $E_R = \hbar^2\pi^2/2ma^2$ is the recoil energy and m is the KRb mass. To study the J

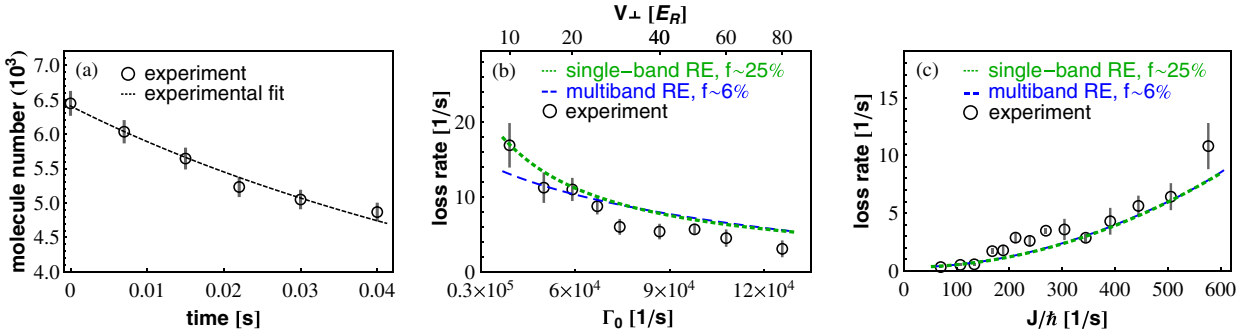

FIG. 2 (color online). (a) Measured number loss of $|\downarrow\rangle$ molecules for an axial (transverse) lattice depth of $V_y = 5E_R$ ($V_\perp = 25E_R$) (circles) and best fit using a rate equation (RE), Eq. (1) (black dashed line). (b) Number loss rate, κ, as a function of Γ_0 (fixing $J \approx 570$ Hz and varying the bare on-site rate via $V_\perp$). (c) Number loss rate, κ, versus J for fixed $\Gamma_0 \approx 87$ kHz (varying V_y and adjusting $V_\perp$ accordingly). V_y ($V_\perp$) was varied from 5 to $16E_R$ (20 to $40E_R$). Black circles are experimental measurements (error bars represent one standard error). Green short-dashed lines show solutions of the RE Eq. (3) using an effective loss rate Γ_{eff} (single-band approximation). The blue long-dashed line shows the multiband RE using $\tilde{\Gamma}_{\text{eff}}$ in Eq. (3). The multiband and single-band RE results were obtained by fixing the filling fraction to be 6%, and 25% respectively. Panels (b) and (c) directly manifest the continuous quantum Zeno effect: in (b) the measured loss rate κ decreases with increasing on-site Γ_0; in (c) a fit to the experimental data supports $\kappa \propto J^2$, with a χ^2 (sum of the squared fitting errors) several times smaller than for a linear fit.

dependence, we vary V_y while simultaneously adjusting $V_\perp$ to keep Γ_0 fixed [Fig. 2(c)]. The loss rate κ is found to depend quadratically on J for fixed Γ_0 and to decrease with increasing Γ_0 for fixed J. This scaling is consistent with the continuous quantum Zeno effect, as we now explain.

Single-band rate equation.—A simple way to understand the loss suppression is to consider two opposite spin particles in a double well, $|\uparrow,\downarrow\rangle$. The left and right sides in this notation represent left and right wells [Fig. 1(b)]. When two molecules occupy the same site the singlet component decays with rate Γ_0, while the decay of the triplet component is suppressed by the centrifugal barrier in odd partial-wave channels [9]. Consequently, the loss rate is determined by $J_s = \sqrt{2}J$, which is the tunneling computed after projecting the initial wave function into the singlet state $|s\rangle = (|\uparrow,\downarrow\rangle - |\downarrow,\uparrow\rangle)/\sqrt{2}$.

When $\hbar\Gamma_0 \gg J_s$, second-order perturbation theory can be applied and gives a net $|\downarrow\rangle$ loss rate of $4\Gamma_{\rm eff}$ with $\Gamma_{\rm eff} = (2(J/\hbar)^2)/\Gamma_0$. This loss rate can be connected to number loss dynamics with a RE, $(dn_{j\downarrow}/dt) = -4q\Gamma_{\rm eff} n_{j+1\uparrow} n_{j\downarrow}$, where $n_{j\downarrow}$ is the number of $|\downarrow\rangle$ molecules at site j and q is the number of nearest neighbor lattice sites ($q = 2$ for tunneling along the tube direction) [18]. Assuming a uniform distribution, the 50:50 mixture implies $n_{j+1\uparrow} = n_{j\downarrow} = n_\downarrow$ and

$$\frac{dn_\downarrow}{dt} = -8\Gamma_{\rm eff}[n_\downarrow(t)]^2 \quad \text{or} \quad \frac{dN_\downarrow}{dt} = -\frac{\kappa_{SB}}{N_\downarrow(0)}[N_\downarrow(t)]^2, \quad (3)$$

where $\kappa_{SB} = 8\Gamma_{\rm eff} n_\downarrow(0)$. All parameters are known except the filling fraction $f = 2n_\downarrow(0)$. The RE assumes that the loss rate depends only on the *average* density. This assumption is valid when the redistribution of density after a loss process occurs faster than the typical time between losses ($J \gg \Gamma_{\rm eff}$) [28].

This simplified single-band model qualitatively reproduces the measured dependence of κ on lattice parameters [green-short-dashed line in Figs. 2(b)–(c)]. However, since Γ_0 is larger than the band gap (e.g., 4 times larger for a $V_y = 5E_R$ and $V_\perp = 40E_R$ lattice), this single-band theory is known to be inadequate. Moreover, in order to fit the experiment, the single-band theory requires $f \approx 25\%$, which is known to be inconsistent with estimates of the filling $f \lesssim 10\%$ from Ramsey spectroscopy procedures [19,29]. Resolution of this discrepancy requires including multiple single-particle bands, which are admixed by strong two-body losses.

Multiband rate equation.— As shown in the Supplemental Material [27], a single-band model overestimates Γ_0, predicting it to be larger than the band gap. Incorporating higher bands decreases Γ_0 and, hence, decreases the f estimated from experiment (since the effective loss rate is inversely proportional to Γ_0). We extract a renormalized effective loss rate by numerically computing the loss of two molecules trapped in a double well along y. We expand the non-Hermitian Hamiltonian $\hat{H} = \hat{H}_0 - i\hbar\beta^{(3D)}\delta_{\rm reg}(\mathbf{r})/2$, where $\delta_{\rm reg}(\mathbf{r}) = \delta(\mathbf{r})(\partial/\partial r)r$ is a regularized pseudopotential [30] and $\hat{H}_0$ the single-particle Hamiltonian, in the 3D Wannier function basis. This model accounts for interaction-mediated band excitations in all three dimensions. We initialize the system with two molecules in the singlet $|s\rangle$ and infer the effective loss rate by fitting the norm decay to $\exp(-4\tilde{\Gamma}_{\rm eff}t)$. Convergence is achieved with 6 bands in each dimension.

Surprisingly, as shown in Figs. 2(b)–(c), both effective loss rates $\Gamma_{\rm eff}$ and $\tilde{\Gamma}_{\rm eff}$ scale similarly with Γ_0 and J. This similarity explains why qualitative experimental signatures of Zeno suppression expected from a single-band model survive even though such a model is invalid. However, the multiband $\tilde{\Gamma}_{\rm eff}$ is $\sim$5 times larger than $\Gamma_{\rm eff}$. Once these effective loss rates are calculated, the only free parameter to fit the experimental measurements is the filling f, which was fixed to be the same for all data shown in Figs. 2(b)–(c). The $\sim$5 times faster loss rate from the multiband model leads to a $\sim$5 times smaller filling fraction of $f = 6\%$ [Figs. 2(b)–(c), blue-long-dashed line] compared to the grossly overestimated 25% extracted using $\Gamma_{\rm eff}$ [Figs. 2(b)–(c) green-short-dashed lines]. The inadequacy of the single-band model to extract the correct filling fraction, and the success of the multiband model, are key results of this work.

Mean-field and DMRG.—The RE, with parameters extracted from the multiband model, describes the experimental observations fairly well at intermediate $V_\perp$, but deviates from them for the largest $V_\perp$. We attribute these deviations to the suppression of tunneling at the cloud's edges due to the energy mismatch between adjacent sites in the harmonic potential generated by the lattice beams. By inhibiting transport, this effect invalidates the assumption that molecules are redistributed rapidly between loss events, and, therefore, the losses are not determined exclusively by the average density but depend on the detailed dynamical redistribution of molecules.

Although this redistribution is absent from the RE, it can be accounted for by solving a master equation with a density matrix, $\hat{\rho}$, projected into the states with at most one molecule per site after adiabatic elimination of doubly occupied states. We keep terms up to order $\Gamma_{\rm eff}$ [17], and we simultaneously account for multiband effects by replacing the single-band $\Gamma_{\rm eff}$ by the renormalized loss rate extracted from the multiband double well solution, obtaining

$$\frac{d}{dt}\hat{\rho} = -\frac{\rm i}{\hbar}[\hat{H}_0, \hat{\rho}] + \mathcal{L}\hat{\rho}. \quad (4)$$

Here, $\hat{H}_0 = -J\sum_{j,\sigma}(\hat{c}^\dagger_{j\sigma}\hat{c}_{j+1\sigma} + \text{H.c.}) + \sum_{j,\sigma} V^\sigma_j \hat{c}^\dagger_{j\sigma}\hat{c}_{j\sigma}$, $\mathcal{L}\hat{\rho} = (1/2)\sum_j [2\hat{A}_j\hat{\rho}\hat{A}^\dagger_j - \hat{\rho}\hat{A}^\dagger_j\hat{A}_j - \hat{A}^\dagger_j\hat{A}_j\hat{\rho}]$ [31], and $V^\sigma_j = (1/2)m\omega^2_\sigma j^2 a^2$ is the parabolic trapping potential felt by molecules in state σ at site j. The average trap frequency $(\omega_\uparrow + \omega_\downarrow)/2$ varies between $\approx 2\pi \times (15 - 40)$ Hz for the experimental range of $V_\perp$. The σ dependence is due to residual differential ac Stark shifts between the two

rotational states. $\mathcal{L}$ is a Lindblad superoperator that accounts for losses, and the jump operators are $\hat{A}_j = \sqrt{2\tilde{\Gamma}_{\rm eff}}[(\hat{c}_{j\uparrow}\hat{c}_{j+1\downarrow} + \hat{c}_{j\uparrow}\hat{c}_{j-1\downarrow}) - (\hat{c}_{j\downarrow}\hat{c}_{j+1\uparrow} + \hat{c}_{j\downarrow}\hat{c}_{j-1\uparrow})]$. We have checked the validity of the renormalized single-band model by confirming that it reproduces the dynamics of the multiband problem for the case of two molecules in four wells.

To solve Eq. (4) we map the hardcore fermions onto hardcore spin-1/2 bosons [32], and then use a mean-field ansatz $\hat{\rho} = \prod_j \tilde{\rho}_j$ with $\tilde{\rho}_j \equiv \sum_{\alpha,\beta=\{\uparrow,\downarrow,0\}} \rho_j^{\alpha,\beta} |\alpha\rangle\langle\beta|$. Here, $\tilde{\rho}_j$ is the reduced projected density matrix at site j, and $\uparrow, \downarrow, 0$ label the three possible local states of spin-up, -down, and the vacuum, respectively. This ansatz leads to closed equations of motion for $\rho_j^{\alpha,\beta}$ (see Supplemental Material [27]). Because of the rapid dephasing of spin coherence resulting from $\omega_\uparrow \neq \omega_\downarrow$, we set $\rho_j^{\sigma,\sigma'\neq\sigma} = 0$, which simplifies the equations further. Although the MF treatment predicts no coherent tunneling for a pure Fock state, we initiate it by assuming nonzero particle-hole coherence $|\rho_j^{\sigma,0}| = 1/2$.

Figure 3(a) shows the dynamics for the largest $V_\perp$, where the coherent tunneling is strongly suppressed by the large parabolic potential $\omega_{\uparrow/\downarrow}$. We see that the dynamics is poorly described by the RE, and the MF solution better describes the data. Admittedly, the MF assumption is an extreme approximation precluding entanglement between parts of the system. In order to test its validity, we also solve Eq. (4) numerically by combining t-DMRG algorithms [20–22] with a stochastic sampling over quantum trajectories [23–25,33]. The results, shown in Fig. 3(b), are converged in the matrix product state dimension $\chi_{\rm MPS}$ and are therefore numerically exact. The differential stark shift for the lattice parameters of Fig. 3 ($\omega_\uparrow/\omega_\downarrow \sim 0.9$) gives rise to an effective spatially dependent magnetic field that disrupts spin correlations generated during the dynamics. In this case the data, t-DMRG, and MF (which explicitly ignores spin correlations) agree up to the times used to extract loss rates from the data, when the contrast has decayed by ~20%. However, in the absence of a differential Stark shift ($\omega_\downarrow = \omega_\uparrow$), we note that the density calculated from t-DMRG saturates at a higher value than predicted by the MF theory, which we attribute to the growth of spin correlations in the absence of dephasing [34].

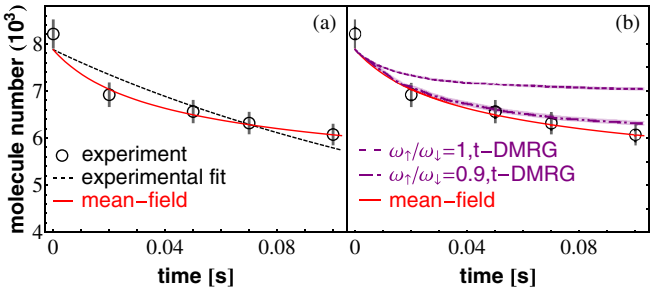

FIG. 3 (color online). Comparison of experimental loss dynamics for the deepest considered lattice to MF and t-DMRG calculations. (a) Molecule loss vs time for $V_\perp = 80E_R$ and $V_y = 5E_R$ [Identical conventions and conditions as Fig. 2(b)]. The MF matches the experimental data better than the RE (experimental fit). (b) Comparison of t-DMRG simulations ($\chi_{\rm MPS} = 128$, 2000 trajectories) to MF, for two different cases: (i) an identical trap for the two spin states with trap frequency $\omega_\downarrow = \omega_\uparrow = 2\pi \times 38$ Hz; and (ii) slightly different trap frequencies $\omega_\downarrow = 2\pi \times 38$ Hz, $\omega_\uparrow = 2\pi \times 34.2$ Hz. Shaded areas indicate the standard error of the mean.

Mean field vs experiment.— With the validity of the MF established, we use it to model the experiment. In the MF calculation, we assume that molecules are initially uniformly distributed within a shell with inner (outer) radius of 20 (50) lattice sites. The shell distribution is expected because molecules are created from a Mott insulator of Rb and a band insulator of K. Assuming only sites with one Rb and one K can yield molecules during STIRAP [7,29], sites in the trap center initially doubly occupied by Rb atoms are lost [7]. We then average over random initial configurations, since the experiments measure an ensemble of 1D tubes. Figures 4(a)–(b) show the MF results (red line), where we used $f = 9\%$ to match the experiment. This is slightly larger than that from the multiband RE (dashed blue line in Fig. 4), $f = 6\%$, since the RE overestimates the loss rate by assuming instantaneous redistribution of the molecules.

Since the molecule distribution in the experiment is known only approximately, we vary the shell width and find that the estimated MF filling fraction that best fits the experimental loss has a range $f \sim 9 \pm 2\%$. The MF accounts better for the dependence of the loss rate on $V_\perp$. Remaining deviations between MF and experiment are seen only for the shallowest $V_\perp$, where the transverse tunneling rate is only 3 times smaller than the axial one, which may indicate the breakdown of 1D dynamics.

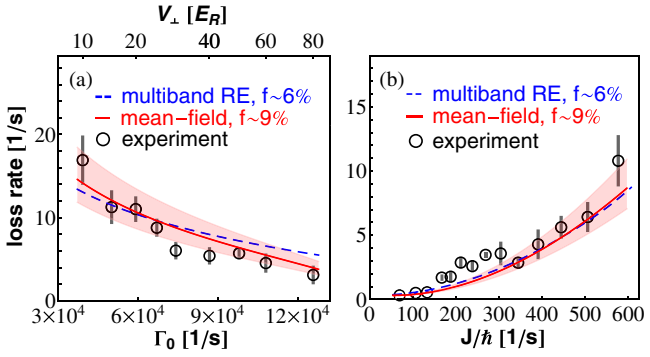

FIG. 4 (color online). (a) Number loss rate, κ, as a function of Γ_0 [same data as Fig. 2(b)]. (b) Number loss rate, κ, vs J for fixed Γ_0 [same data as Fig. 2(c)]. Black circles are experimental measurements. Blue long-dashed and solid red lines show RE and MF solutions, respectively, using $\tilde{\Gamma}_{\rm eff}$ (multiband model). The shaded area accounts for $\pm 2\%$ variations around the MF estimate of $f \sim 9\%$ arising from the uncertainty in the initial molecule distribution.

Conclusions.—The understanding of the underlying physical mechanism responsible for the loss suppression in KRb opens the path for laboratory explorations of iconic models of quantum magnetism combining motional and spin degrees of freedom, previously believed to be inaccessible due to losses. These include the extended t-J model, predicted to exhibit itinerant ferromagnetism, d-wave superfluidity [35,36], and topological phases [3,37]. Our findings also extend to other dissipative systems, such as alkaline earth atoms [38–41] and other chemically reactive molecular species [42].

The authors thank A. Daley for useful discussions and acknowledge funding from NIST, JILA-NSF-PFC-1125844, NSF-PIF, ARO, ARO-DARPA-OLE, and AFOSR. K. R. A. H., B. G. and M. F.-F. thank the NRC postdoctoral fellowship program for support. S. A. M. and J. P. C. acknowledge funding from NDSEG. A. M. R. and K. R. A. H. thank the KITP for its hospitality. This work utilized the Janus supercomputer, supported by NSF, NCAR, and CU.

*arey@jilau1.colorado.edu

[1] C. Trefzger, C. Menotti, B. Capogrosso-Sansone, and M. Lewenstein, J. Phys. B **44**, 193001 (2011).
[2] M. Baranov, M. Dalmonte, G. Pupillo, and P. Zoller, Chem. Rev. **112**, 5012 (2012).
[3] T. Lahaye, C. Menotti, L. Santos, M. Lewenstein, and T. Pfau, Rep. Prog. Phys. **72**, 126401 (2009).
[4] D. DeMille, Phys. Rev. Lett. **88**, 067901 (2002).
[5] T. Zelevinsky, S. Kotochigova, and J. Ye, Phys. Rev. Lett. **100**, 043201 (2008).
[6] L. D. Carr, D. DeMille, R. V. Krems, and J. Ye, New J. Phys. **11**, 055049 (2009).
[7] S. Ospelkaus, K.-K. Ni, D. Wang, M. De Miranda, B. Neyenhuis, G. Quéméner, P. Julienne, J. Bohn, D. S. Jin, and J. Ye, Science **327**, 853 (2010).
[8] K.-K. Ni, S. Ospelkaus, D. Wang, G. Quéméner, B. Neyenhuis, M. De Miranda, J. Bohn, J. Ye, and D. S. Jin, Nature (London) **464**, 1324 (2010).
[9] M. De Miranda, A. Chotia, B. Neyenhuis, D. Wang, G. Quéméner, S. Ospelkaus, J. Bohn, J. Ye, and D. S. Jin, Nat. Phys. **7**, 502 (2011).
[10] B. Yan, S. A. Moses, B. Gadway, J. P. Covey, K. R. A. Hazzard, A. M. Rey, D. S. Jin, and J. Ye, Nature (London) **501**, 521 (2013).
[11] N. Syassen, D. Bauer, M. Lettner, T. Volz, D. Dietze, J. García-Ripoll, J. Cirac, G. Rempe, and S. Dürr, Science **320**, 1329 (2008).
[12] M. J. Mark, E. Haller, K. Lauber, J. G. Danzl, A. J. Daley, and H.-C. Nägerl, Phys. Rev. Lett. **107**, 175301 (2011).
[13] B. Misra and E. C. G. Sudarshan, J. Math. Phys. (N.Y.) **18**, 756 (1977).
[14] W. M. Itano, D. J. Heinzen, J. J. Bollinger, and D. J. Wineland, Phys. Rev. A **41**, 2295 (1990).
[15] M. C. Fischer, B. Gutiérrez-Medina, and M. G. Raizen, Phys. Rev. Lett. **87**, 040402 (2001).
[16] Y.-J. Han, Y.-H. Chan, W. Yi, A. J. Daley, S. Diehl, P. Zoller, and L.-M. Duan, Phys. Rev. Lett. **103**, 070404 (2009).
[17] J. J. García-Ripoll, S. Dürr, N. Syassen, D. Bauer, M. Lettner, G. Rempe, and J. Cirac, New J. Phys. **11**, 013053 (2009).
[18] S. K. Baur and E. J. Mueller, Phys. Rev. A **82**, 023626 (2010). [We note that in this reference there is a factor of 2 missing on the right-hand side of Eq. (13)].
[19] K. R. A. Hazzard, S. R. Manmana, M. Foss-Feig, and A. M. Rey, Phys. Rev. Lett. **110**, 075301 (2013).
[20] G. Vidal, Phys. Rev. Lett. **93**, 040502 (2004).
[21] A. J. Daley, C. Kollath, U. Schollwöck, and G. Vidal, J. Stat. Mech. (2004) P04005.
[22] S. R. White and A. E. Feiguin, Phys. Rev. Lett. **93**, 076401 (2004).
[23] H. Carmichael, *An Open Systems Approach to Quantum Optics, Lectures Presented at the Université Libre de Bruxelles*, Lecture Notes in Physics monographs (Springer, Berlin, 1991).
[24] K. Mølmer, Y. Castin, and J. Dalibard, J. Opt. Soc. Am. B **10**, 524 (1993).
[25] R. Dum, A. S. Parkins, P. Zoller, and C. W. Gardiner, Phys. Rev. A **46**, 4382 (1992).
[26] B. Neyenhuis, B. Yan, S. A. Moses, J. P. Covey, A. Chotia, A. Petrov, S. Kotochigova, J. Ye, and D. S. Jin, Phys. Rev. Lett. **109**, 230403 (2012).
[27] See Supplemental Material at http://link.aps.org/supplemental/10.1103/PhysRevLett.112.070404 for details of our multiband calculation of effective parameters and various numerical treatments of loss dynamics.
[28] Note: Although a transition dipole matrix element exists between $|\uparrow\rangle$ and $|\downarrow\rangle$, we neglect dipolar interactions because of the lack of spin coherence in our 50:50 mixture.
[29] A. Chotia, B. Neyenhuis, S. A. Moses, B. Yan, J. P. Covey, M. Foss-Feig, A. M. Rey, D. S. Jin, and J. Ye, Phys. Rev. Lett. **108**, 080405 (2012).
[30] K. Huang and C. N. Yang, Phys. Rev. **105**, 767 (1957).
[31] Note: The sums run over all lattice sites, operators acting outside the bounds are implicitly ignored.
[32] H. Tsunetsugu, M. Sigrist, and K. Ueda, Rev. Mod. Phys. **69**, 809 (1997).
[33] J. Schachenmayer, L. Pollet, M. Troyer, and A. J. Daley, Phys. Rev. A **89**, 011601 (2014).
[34] M. Foss-Feig, A. J. Daley, J. K. Thompson, and A. M. Rey, Phys. Rev. Lett. **109**, 230501 (2012).
[35] A. Gorshkov, M. Hermele, V. Gurarie, C. Xu, P. Julienne, J. Ye, P. Zoller, E. Demler, M. Lukin, and A. Rey, Nat. Phys. **6**, 289 (2010).
[36] K. A. Kuns, A. M. Rey, and A. V. Gorshkov, Phys. Rev. A **84**, 063639 (2011).
[37] M. A. Baranov, K. Osterloh, and M. Lewenstein, Phys. Rev. Lett. **94**, 070404 (2005).
[38] A. D. Ludlow, N. D. Lemke, J. A. Sherman, C. W. Oates, G. Quéméner, J. von Stecher, and A. M. Rey, Phys. Rev. A **84**, 052724 (2011).
[39] M. Bishof, M. J. Martin, M. D. Swallows, C. Benko, Y. Lin, G. Quéméner, A. M. Rey, and J. Ye, Phys. Rev. A **84**, 052716 (2011).
[40] A. Traverso, R. Chakraborty, Y. N. Martinez de Escobar, P. G. Mickelson, S. B. Nagel, M. Yan, and T. C. Killian, Phys. Rev. A **79**, 060702 (2009).
[41] C. Lisdat, J. S. R. V. Winfred, T. Middelmann, F. Riehle, and U. Sterr, Phys. Rev. Lett. **103**, 090801 (2009).
[42] P. S. Żuchowski and J. M. Hutson, Phys. Rev. A **81**, 060703 (2010).